Intriguing Mass Spectrometric Behavior of Guanosine Under Low Energy Collision-Induced Dissociation: H_2O Adduct Formation and Gas-Phase Reactions in the Collision Cell

Robin Tuytten, Filip Lemière,* Walter Van Dongen,* and Eddy L. Esmans*
Department of Chemistry, Nucleoside Research Unit and Center for Mass Spectrometry and Proteomics, University of Antwerp, Antwerp, Belgium

Erwin Witters
Department of Chemistry and Cryospectroscopy, University of Antwerp, Antwerp, Belgium

Wouter Herrebout and Benjamin Van Der Veken
Department of Chemistry, Cryospectroscopy, University of Antwerp, Antwerp, Belgium

Ed Dudley and Russell P. Newton
Biochemistry Group, School of Biological Sciences and Biomolecular Analysis Mass Spectrometry Facility, University of Wales, Swansea, United Kingdom

An in-depth study of the fragmentation pathway of guanosine was conducted by using an in-source collision-induced dissociation high-mass accuracy tandem mass spectrometry experiment. The equivalent of MS^4 data, a level of information normally achieved on ion trap instruments, was obtained on a Q-TOF mass spectrometer. The combination of the features of high-resolution, accuracy, and in-source CID permitted the unambiguous elucidation of the different fragmentation pathways. Furthermore the elemental compositions of the product ions generated were assigned and their mutual genealogical relationships established. Formerly proposed dissociation pathways of guanosine were revisited and elaborated on more deeply. Furthermore, the presence of H_2O in the collision cell of several tandem MS instruments was demonstrated and its effect on the product ion spectra investigated. The neutral gain of H_2O by particular fragments of guanosine was experimentally proven by using argon, saturated with $H_2^{18}O$, as the collision gas. Data indicating the occurrence of more complex reactions in the collision cell as a result of the presence of H_2O were produced, specifically relating to neutral gain/neutral loss sequences. In silico calculations supported the experimental observation of neutral gain by guanosine fragments and predicted a similar behavior for adenosine. The latter was subsequently experimentally confirmed. (J Am Soc Mass Spectrom 2005, 16, 1291–1304) © 2005 American Society for Mass Spectrometry

Nucleosides have been established as molecules of exceptional importance in biochemical research for a long period. They are the building blocks of the macromolecules RNA and DNA, exogeneous nucleoside analogs are used as anti(retro)viral and anticancer agents [1], and nucleoside levels in urine have the potential to act as cancer biomarkers [2–5]. As their occurrence is both ubiquitous and quantitatively varying [6, 7] their unequivocal characterization is crucial.

For guanine alone over 20 natural variants are known to occur in RNA [6], which makes structural identification a challenging task.

In our earlier LC-ESI-MS/MS experiments of urinary nucleosides [8], unexpected product ions of guanosine and its methylated derivatives were detected. The presence of these ions prompted us to perform additional mass spectrometric studies since their origin was not straightforward. This report provides an in-depth study of the fragmentation behavior of guanosine under low-energy CID conditions, revealing H_2O addition to specific fragments.

We also wish to demonstrate the use of a Q-TOF mass spectrometer in the collection of the equivalent of MS^4 data, a level of information normally acquired only in ion trap- or FT-MS^n experiments [9, 10]. This was achieved by making optimal use of "in-source" CID,

Published online June 23, 2005

Address reprint requests to Dr. E. L. Esmans, Department of Chemistry, University of Antwerp, Groenenborgerlaan 171, B-2020 Antwerp, Belgium. E-mail: Eddy.Esmans@ua.ac.be

* Also at the Center for Mass Spectrometry and Proteomics, University of Antwerp, Belgium.

© 2005 American Society for Mass Spectrometry. Published by Elsevier Inc.
1044-0305/05/$30.00
doi:10.1016/j.jasms.2005.03.026

Received December 17, 2004
Revised March 18, 2005
Accepted March 24, 2005

yielding product ions up to the third generation, which subsequently could be studied in low-energy CID experiments (MS^4). Additionally, the high selectivity and high mass accuracy of the Q-TOF instrument made the assignment of elemental compositions possible [11].

These extraordinary features of the Q-TOF were field-tested in the further elucidation of the fragmentation behavior of guanosine under low-energy CID conditions. The first data on the accurate mass values of many of the guanosine fragments were collected, then the structure of many product ions previously reported were confirmed or revised, and new product ions were identified. As a result, the unambiguous disentanglement of major fragmentation pathways was possible, as the product ions at the top of the genealogical relationships were already produced in source and afterwards selected by the quadrupole filter. The detailed elucidation of the fragmentation patterns of guanosine will greatly aid in the development of successful MS strategies allowing the discrimination of isomeric methylated guanosines, a current topic of heightened research interest [12–14].

The thorough analysis of the observed data revealed the importance of the presence of H_2O in the collision cell of tandem MS instruments. This presence was proven by the availability of accurate mass data and by doping the collision gas with $H_2^{18}O$. The occurrence of H_2O in the collision cell accounts for many of the previously nonassigned product ions of guanosine and also triggers many neutral gain/neutral loss sequences involving H_2O and NH_3. Additionally, it was shown that the presence of H_2O was not an artefact but a feature inherent of many set-ups.

Recently, in silico studies concerning the stability of microsolvated guanine [15–17] and the solvent mediated tautomerization of purine [18] were published. Our in silico calculations supported the ability of particular product ions to gain a neutral molecule of H_2O. The calculations also showed hydrogen bonding to be the driving force for the formation of stable complexes. Additionally, our calculations suggested that the neutral gain of H_2O was not a unique feature of some particular product ions of guanosine (and its methylated derivatives) [8, 19], as it was also predicted for some product ions of adenosine. Our experiments indeed showed a similar H_2O gain in the collision cell for some adenosine fragments.

Experimental

Chemicals

Guanosine and adenosine were purchased from Sigma (St. Louis, MO). Deuterated water, D_2O, (D, 99.7%) and ^{18}O-labeled water, $H_2^{18}O$, (^{18}O, 95%) were obtained from Cambridge Isotope Laboratories, Inc. (Adover, MA), and methanol-d, CH_3OD, (D, +99.5%) from Aldrich Chemical Company, Inc. (Milwaukee, WI). Methanol (HPLC grade) and phosphoric acid were acquired from Acros Organics (Geel, Belgium). H_2O (HPLC grade) was purchased from Fischer Scientific (Loughborough, Leicestershire, UK). Formic acid (99–100%; ultra pure) was purchased from VWR international (Leuven, Belgium). The argon (Alphagaz 1: $H_2O < 3$ ppm, $O_2 < 2$ ppm, $C_nH_m < 0.5$ppm) used as the collision gas in the CID experiments was supplied by L'Air Liquide (Luik, Belgium). The argon used to prepare the $H_2^{18}O$ doped argon had a purity of 99.9999% (Alphagaz 2: $H_2O < 0.5$ ppm, $O_2 < 0.1$ ppm, $C_nH_m < 0.1$ ppm) and was also purchased from L'Air Liquide.

One mL stock standard solutions of 10^{-3}M of guanosine and adenosine were prepared in 50:50 CH_3OH/H_2O or 50:50 CH_3OD/D_2O (only guanosine). Working solutions were obtained by diluting the stocks further to 10^{-5}M in 50:49.9:0.1 CH_3OH/H_2O/HCOOH (vol/vol) or 50:49.9:0.1 CH_3OD/D_2O/HCOOH (vol/vol). For this purpose, a 10% formic acid solution in H_2O or D_2O was used.

Gas mixtures of argon doped with $H_2^{18}O$ were obtained as follows: A Swagelok DOT-3E1800 (Swagelok, Solon, OH) stainless steel gas cylinder was connected to a pressure manifold [20]°and°evacuated,°the°final°pressure being less than 10^{-3} mbar. Then a small amount of $H_2^{18}O$ vapor was added and the surface of the gas cylinder was passivated. This procedure was repeated several times. Finally, an additional amount of $H_2^{18}O$ was added and mixed with a large excess of argon. The amount of $H_2^{18}O$ was estimated to be ca. 2300 ppm. During all experiments, exchanges were observed between the $H_2^{18}O$ molecules present in the argon and $H_2^{16}O$ molecules adsorbed on the stainless steel connections of the mass spectrometer. The resulting $H_2^{16}O/H_2^{18}O$ ratio, derived from the different mass spectra, varied roughly between 0.25 and 1.5.

Instrumentation and MS Conditions

A Q-TOF II mass spectrometer (Waters, Manchester, UK) equipped with a standard pneumatically assisted electrospray probe and a Z-spray source (Waters) was used to perform this study. Electrospray spectra were recorded in the positive ion mode. The applied ionization voltage was 3.3 kV, the source and desolvation temperature were both set at 80 °C. A cone gas flow rate of ca. 60L/h and a desolvation gas flow rate of ca. 150L/h were applied. The 10^{-5}M guanosine solutions were infused at a flow rate of 10 μL/min by a syringe pump (Harvard Apparatus, Natick, MA). Argon was used as the collision gas for the MS/MS experiments. For both the standard argon and the $H_2^{18}O$ doped argon, the gas pressure reducing valves of the supply cylinders were tuned until the readout for the collision cell gas pressure on the instrument was ca. 10 psi. For product ion spectra, the precursor ions were selected at unit resolution, adequately removing isotopic species from the spectrum. Furthermore, the product ion spectra were examined at low collision energies to confirm the isotopic purity of the precursor ion. Scan time and

Table 1. Applied experimental conditions for the different ionic species subjected to MS/MS.

	m/z	CV (V)	CE-range (eV)	Time/CE (min)
$[MH]^+$	284	20	5–50	1.3/2*
$[BH_2]^+$	152	40	5–50	1.3/2*
$[BH_2]^+ - NH_3$	135	65	5–25	3
$[BH_2]^+ -$ NHCNH	110	65	5–25	3
$[BH_2]^+ -$ HNCO	109	65	5–25	5
$[BH_2]^+ - NH_3 + H_2O$	153	65	5–35	3
$[BH_2]^+ -$ NHCONH $+ H_2O$	128	65	5–25	3

*Applied for the $H_2^{18}O$-doped Argon experiments

inter-scan time were 1.0 and 0.1 s, respectively. The data were processed using MassLynx software suite version 3.5 (Waters, Manchester, UK).

For high mass accuracy, the Q-TOF was calibrated using 0.1% phosphoric acid in 50:50 MeOH/H_2O (vol/vol). The instrument drift was compensated by applying a lock mass correction. Depending on the experiment, protonated guanosine $[MH]^+$ (*m/z* 284.0995), the protonated base $[BH_2]^+$ (*m/z* 152.0572), or other product ions were used as lock mass. In the latter case only the fragments for which the elemental composition was confirmed by us and others (*m/z* 135.0307, *m/z* 110.0354, *m/z* 93.0089, *m/z* 82.0405, and *m/z* 80.0249) were utilized.

For the in-source CID experiments it was necessary to optimize the cone voltage for each of the ions of interest. A 10^{-5}M guanosine solution was infused at 10 μL/min and full scan spectra were recorded (*m/z* 100–600) with a cone voltage varying between 5 and 80 V (at 5 V intervals each 30 s). The optimal cone voltage (CV) for each relevant ion was selected upon the evaluation of the extracted ion chromatograms and the corresponding spectra (cf. isobaric interferences) and are summarized in Table 1. With these values the energy resolved spectra of $[MH]^+$, $[BH_2]^+$, and the other ions of interest were recorded. The collision energy (CE) was varied in intervals of 5 eV with a starting value set at 5 eV (Table 1). The accumulation times used for each CE setting are summarized in Table 1. The TOF analyzer was programmed to record the *m/z* range 50–400 for guanosine and the *m/z* range 50–250 for $[BH_2]^+$ and the other ionic species studied.

Computational Details

Density functional theory (DFT) calculations were performed using Gaussian 03 [21]. For all calculations, Becke's three parameter exchange functional [22] was used in combination with the LYP correlation functional [23], while the 6-31+G(d,p) basis set was used throughout. To reduce errors arising from the numerical integration for all calculations, the *finegrid* option, corresponding to roughly 7000 grid points per atom, was used.

Results and Discussion

As a starting point for this study, the energy resolved spectra under low-energy CID conditions of the protonated molecule $[MH]^+$ (*m/z* 284) of guanosine were recorded. Apart from a small contribution of D-ribose fragments all products were derived from $[BH_2]^+$. Therefore, the cone voltage was optimized for the in-source generation of the protonated base $[BH_2]^+$, and its energy-resolved spectra were recorded (Scheme **1**). [The D-ribose related ions $C_3H_5O^+$ (calc. *m/z* 57.0340; meas. *m/z* 57.0339) and $C_3H_3O_2^+$ (calc. *m/z* 71.0133; meas. *m/z* 71.0123) were omitted from Scheme **1**.] This resulted in more than 20 product ions. Most of them were present when applying a CE of 35 eV (see Figure 1). Most product ions were measured with an accuracy within 0.5 mDa (some low abundant ions within 1.6 mDa) (cf. Scheme **1**). These data were compared with the data found in earlier studies, more particularly in the excellent CID study of protonated guanine by Gregson and McCloskey [24], and our accurate mass data confirmed their identity. However, several product ions found by us were not reported before. Most intriguing was the observation of ions solely associated with $[BH_2]^+$ but at *m/z* values higher than the actual *m/z* value of $[BH_2]^+$ itself.

To confirm and to expand the different known fragmentation schemes the cone voltages were optimized for the in-source generation of the main product ions of $[BH_2]^+$. This allowed us to record the (energy resolved) spectra of these species as fourth generation ions (MS^4). Using this approach, we felt confident that we would be able to assign most of the generated product ions to one of the two main fragmentation pathways observed for $[BH_2]^+$, i.e., the $[BH_2]^+ - NH_3$, and the $[BH_2]^+ -$ HNCNH pathways [24] starting at *m/z* 135 and 110, respectively. At the same time a third—but minor—pathway, involving the expulsion of a HNCO from the $[BH_2]^+$ ion leading to a product ion at *m/z* 109, was studied.

These "pseudo" MS^4 data have to be interpreted carefully: because of the nondiscriminating environment in the source, isobaric interferences cannot be ruled out. However, in most cases it was sufficient to compare the MS^4 spectral data with the product ion spectra of the previously generated ions, i.e., $[BH_2]^+$ or even $[MH]^+$. The eventual presence of such isobaric interferences would result in product ions absent in the previously recorded spectra.

Collision-Induced Dissociation of In-Source Formed Ions with m/z Values 135, 110, and 109

The $[BH_2]^+ - NH_3$ pathway: low-energy CID of m/z 135. To study the fragmentation behavior of *m/z* 135 more in depth, this ion was generated in source of the Q-TOF mass spectrometer using a cone voltage of 65 V. Monoisotopic *m/z* 135 was selected by the quadrupole filter and accurate mass energy-resolved spectra were

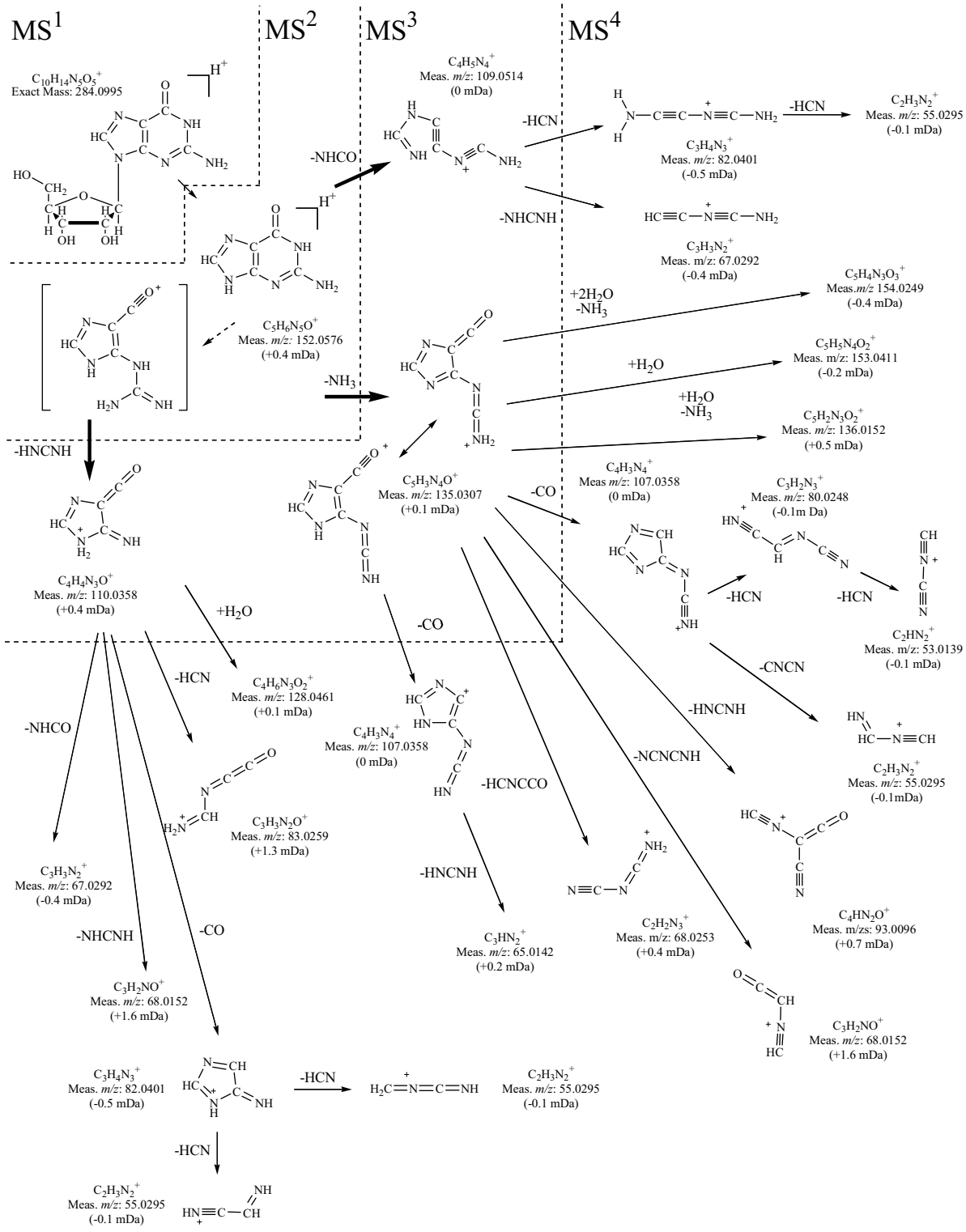

Scheme 1. Dissociation scheme of $[MH]^+$, based on the energy resolved spectra of $[MH]^+$ and $[BH_2]^+$. The measured *m/z* values were indicated after lock mass correction. The deviation compared with the calculated *m/z* is given (mDa). Only those product ions which were also present in the product ion spectra of the ions at *m/z* 135, 110, and 109 are included.

collected in a range of 5–25 eV (e.g., Figure 2 CE 20). Starting from the ring-opened intermediate, this ion could be explained by the loss of NH_3. The accurate mass data of the product ions of *m/z* 135 confirm the elemental compositions of the ions presented in Scheme 1.

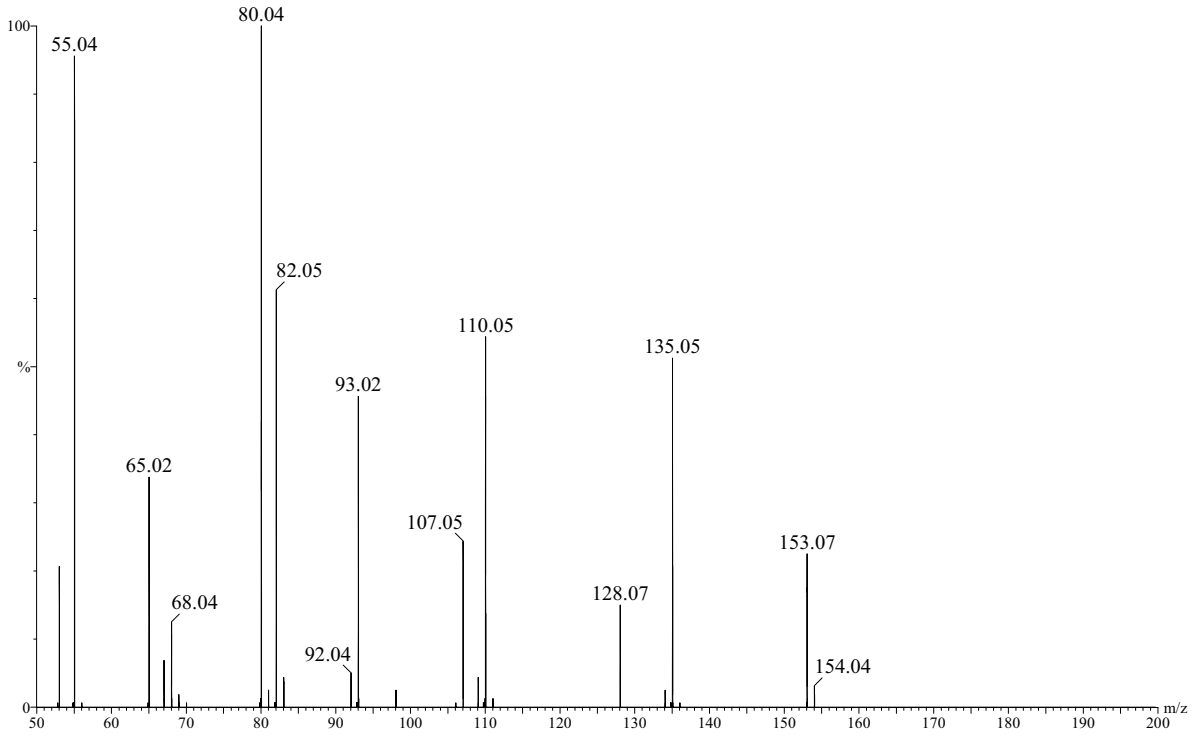

Figure 1. Product ion spectrum of the in-source formed $[BH_2]^+$ ion at *m/z* 152 (CV 40 V and CE 35 eV; no lock mass correction, uncentered).

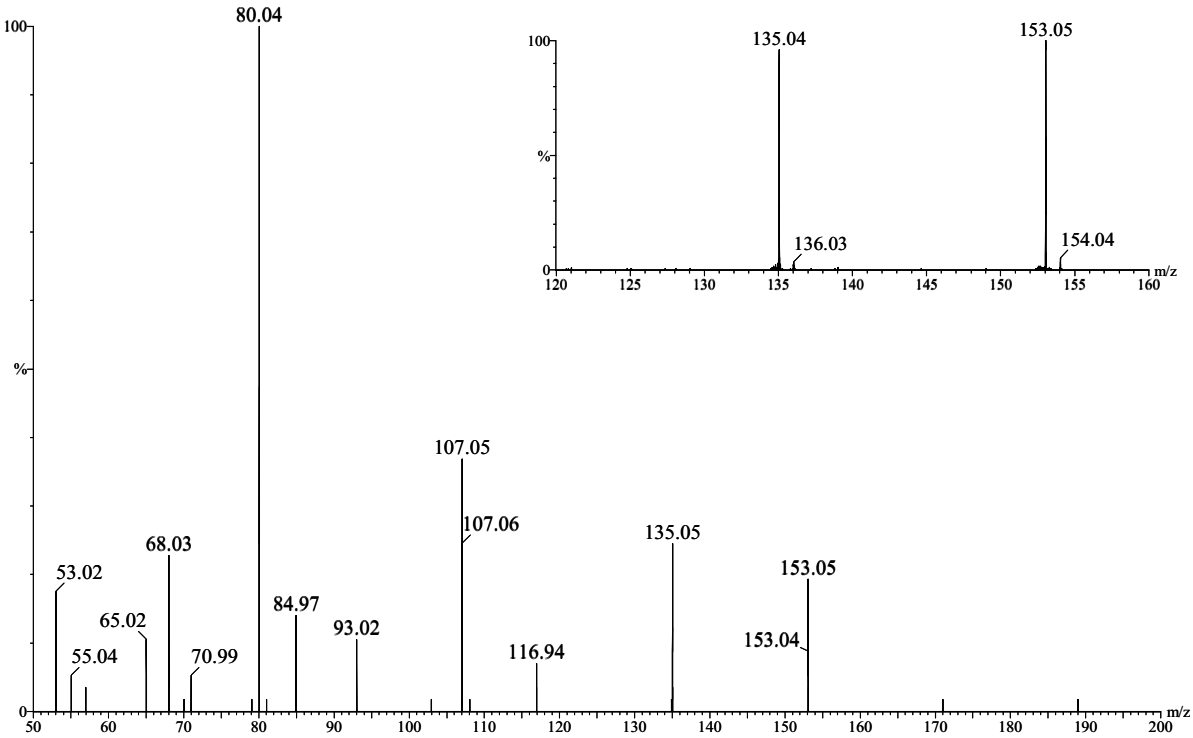

Figure 2. Product ion spectrum of the in-source formed ion at *m/z* 135 (CV 65 V and CE 20 eV; no lock mass correction, uncentered). The inset shows a detail of the product ion spectrum of *m/z* 135 at low CE (CV: 65 V and CE: 5 eV).

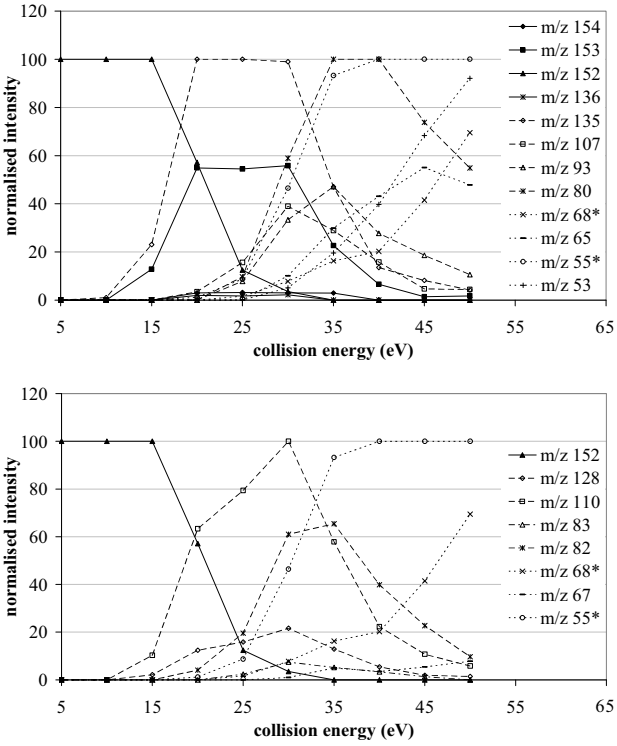

* These productions are present in both pathways.

Figure 3. Energy resolved mass spectra of $[BH_2]^+$: the "deammoniation pathway" (*m/z* 135) (upper panel) and the "loss of a cyanamide pathway" (*m/z* 110) (lower panel).

As already seen for the product ions of the $[BH_2]^+$ ion (Figure 1), additional product ions at masses above the precursor ion were observed (*m/z* 154, 153, and 136) after initial selection of *m/z* 135. At a CE of 5 eV, *m/z* 153 is even more prominent than the precursor ion *m/z* 135 itself (inset Figure 3). Comparison of the elemental composition of *m/z* 153 ($C_5H_5N_4O_2^+$) and *m/z* 135 ($C_5H_3N_4O^+$) suggested the addition of H_2O. This was confirmed when the actual measured mass difference between the two *m/z* values was checked (Δm = 18.0105), which is in good agreement with the elemental composition H_2O (calc. mass: 18.0106).

The ions at *m/z* 154 (calc. $C_5H_4N_3O_3^+$) and 136 (calc. $C_5H_2N_3O_2^+$), product ions of *m/z* 135, were not as prominent as the H_2O adduct at *m/z* 153, but were also present in both the energy resolved spectra of guanosine $[MH]^+$ and the intact base moiety $[BH_2]^+$. These ions needed the addition of two H_2O molecules, and were studied in more detail using ^{18}O labeling (*vide infra*).

With increasing CE, some product ions were detected which were formerly not associated with the deammoniation pathway. Under high resolution conditions a doublet was found at *m/z* 68 ($C_2H_3N_2^+$, calc. *m/z* 68.0249; meas. *m/z* 68.0267 and $C_3H_2NO^+$, calc. *m/z* 68.0136; meas. *m/z* 68.0109). In the literature (low-resolution conditions) this ion at *m/z* 68 was associated solely with the $[BH_2]^+$ – HNCNH pathway [24]. In our MS/MS spectra of *m/z* 110, only a very low abundant ion at *m/z* 68 (calc. *m/z* 68.0136; meas. *m/z* 68.0120) was found; therefore the formation of the product ion at *m/z* 68 probably proceeded primarily via the $[BH_2^+] - NH_3$ pathway (via *m/z* 135) and not via the $[BH_2]^+$ – HNCNH pathway (via *m/z* 110). This was also more in agreement with Gregson's ^{15}N isotope labeling experiments [24].

Another product ion was found at *m/z* 55 with elemental composition $C_2H_3N_2^+$ (calc. *m/z* 55.0296; meas. *m/z* 55.0308). The occurrence of this product ion in the fragmentation pathway of *m/z* 135 could also shed another light on previous data, as will be discussed in the next paragraph.

The $[BH_2]^+$ – HNCNH pathway: low-energy CID of m/z 110. In analogy with the experiments described above for *m/z* 135, *m/z* 110 was generated in source as a result of the loss of cyanamide from $[BH_2]^+$. The product ions recorded after the dissociation of *m/z* 110 were also summarized in Scheme 1.

The most remarkable product ion resulting from the low-energy CID of *m/z* 110 was *m/z* 128, again a fragment with a higher *m/z* -value than the actual parent ion. With this product ion the elemental composition $C_4H_6N_3O_2^+$ was associated. Once more this suggested the addition of H_2O to *m/z* 110 ($C_4H_4N_3O^+$).

In general the elemental compositions of the other fragments were identical to previously reported data [24, 25]. The presence of *m/z* 83 was also noticed in the energy resolved spectra of *m/z* 110 ($C_3H_3N_2O^+$) (calc. *m/z* 83.0245; meas. *m/z* 83.0247). This ion could tentatively be explained by the direct loss of HCN from the ion at *m/z* 110. To the best of our knowledge this fragment was not reported in earlier CID fragmentation studies of guanosine. A further previously unreported low abundant product ion appeared at higher CE-values, at *m/z* 67 with a calculated elemental composition $C_3H_3N_2^+$ (calc. *m/z* 67.0296; meas. *m/z* 67.0294).

The ion at *m/z* 55 was already reported before as a product in the $[BH_2]^+$-HNCNH pathway. However, our approach of selecting the initial ions of the respective dissociation pathways showed that there was an alternative way to form *m/z* 55, i.e., as a product ion of *m/z* 107 in the $[BH_2]^+$-NH_3-pathway (*vide supra*). Both pathways were not recognized in the past and were in agreement with previously published ^{15}N-labeling data [24].

The $[BH_2]^+$ - HNCO pathway: low-energy CID of m/z 109. A third mechanism of initial dissociation of guanosine was recently proposed by Kamel and Munson [25]. It involved the loss of HCNO out of the $[BH_2]^+$ leading to a fragment at *m/z* 109 ($C_4H_5N_4^+$ calc. *m/z* 109.0514; meas. *m/z* 109.0514).

In our energy resolved spectra of $[BH_2]^+$, this product ion also appeared but at low abundance. Notwithstanding its minor abundance, it was possible to generate enough of *m/z* 109 by in-source CID to record its

energy resolved spectra. Three new product ions were found as summarized in Scheme 1. Unlike the other progenitor ions *m/z* 135 and *m/z* 110 of the other dissociation pathways, no product ions above the actual parent ion were seen.

The energy resolved spectra of the main dissociation pathways potentially arising from $[BH_2]^+$ are summarized in Figure 3. The $[BH_2]^+ - HNCO$ pathway starting from *m/z* 109 was omitted as it was far less abundant compared with the other two. Only the product ions which appeared both in the energy resolved spectra of $[BH_2]^+$ and the spectra of the progenitors of the respective dissociation pathway were depicted.

The ions at *m/z* 68 and 55 were common to both main dissociation pathways; however, the energy resolved spectra of the ions at *m/z* 135 and 110 suggested that the major contribution to *m/z* 68 followed the fragmentation pattern starting from *m/z* 135, while the major contribution to *m/z* 55 mainly ensued from the dissociation of *m/z* 110.

The ions at *m/z* 134 and 92 are not yet accounted for. In contrast to literature data, direct decarbonylation of the $[BH_2]^+$ was not observed as reported by Gregson et al. [24]; instead, loss of HNCO was found. No straightforward explanation could be given. The only significant difference was the nature of the collision gas (argon versus xenon).

Study of the H_2O Addition in the Collision Cell

Neutral gain of H_2O by the product ions m/z 135 and 110. The accurate and elemental composition data presented above point towards the neutral gain of H_2O by the fragments *m/z* 110 and 135 in the collision cell, although the presence of H_2O in the collision cell was not recognized. In the following experiments only a mono-isotopic ion was permitted to pass the quadrupole filter (unit resolution), and argon was used for CID (H_2O content <3ppm).

To prove that the neutral gain of H_2O only took place in the collision cell, one should rule out the contribution of the ionization source as a hypothetical source of H_2O, since electrospray ionization was performed under atmospheric conditions (moisture) and guanosine was presented to the mass spectrometer in a MeOH/H_2O (0.1% FA) solution. Neutral gain of H_2O or MeOH was already briefly mentioned in an APCI ion trap MS study for fragments of some nucleobases (except guanine) [26], and addition of acetonitrile to benzyl cations was monitored in a ion trap mass spectrometer [27]. In both cases the solvent molecules were provided during passage from the source into the MS.

To check eventual source contributions, guanosine was infused in a MeOD/D_2O (0.1% FA) solution. By doing so the H_2O at the entrance of the mass spectrometer was effectively replaced by D_2O. If any neutral gain of H_2O in the collision cell should originate from the ion source, a neutral gain of D_2O should be anticipated. Under these circumstances we were able to create a $[d^3 - BD_2]^+$ ion (*m/z* 157) by in-source CID. The latter was monoisotopically selected by the quadrupole filter and exposed to CID. At low collision energy (e.g., 5eV) it was noticed that the precursor ion was exchanging deuterium (D^+) for hydrogen (H^+), resulting in a *m/z* shift of −1 u. This indicated the presence in the collision cell of a species capable of exchanging protons, e.g., H_2O.

The ions detected at *m/z* 110 and 135 were now found at *m/z* 113 and 137. This was in full agreement with the structures of the ions containing 3 and 2 exchangeable protons, respectively, (see also Table 2).

Furthermore, ions were also detected at *m/z* 131 and 155 corresponding to the uptake of H_2O (Δm 18). These data excluded the electrospray source as the supplier of H_2O molecules to the collision cell. In addition, the collection of the energy resolved spectra of $[d^3 - BD_2]^+$ and the corresponding deuterated progenitors of the dissociation pathways lead to an extra confirmation of the proposed pathways as depicted in Scheme 1. The accurate mass values are summarized in Table 2.

More proof of the neutral gain of H_2O in the collision cell was found in an experiment where the argon gas was doped with $H_2^{18}O$. Accurate mass energy resolved spectra were recorded for the $[MH]^+$ of guanosine and the in-source formed $[BH_2]^+$, *m/z* 135 and 110 ions. Figure 4 shows the product ion spectrum of the in-source formed BH_2^+ ion (*m/z* 152) recorded at CE 35 eV.

Under these circumstances, new ions arose at *m/z* 155 and 130 which were highly significant: they were observed in both the product ion spectra of $[BH_2]^+$ and the product ion spectra of *m/z* 135 and 110, respectively. Interpretation of the accurate mass data lead to following elemental compositions $C_5H_5N_4^{16}O^{18}O^+$ (calc. *m/z* 155.0455; meas. *m/z* 155.0457) and $C_4H_6N_3^{16}O^{18}O^+$ (calc. *m/z* 130.0502; meas. *m/z* 130.0512) corresponding with $H_2^{18}O$ adducts of *m/z* 135 and 110, respectively. As such, it is indisputably proven that these product ions can undergo neutral gain of H_2O in the collision cell.

As these product ions reacted with H_2O in the collision cell, there was ample reason to believe that this process could also occur in the electrospray source. By optimizing the CV it was possible to generate these H_2O adducts in the ion source and to subject them to CID analysis in the collision cell. From the energy resolved spectra of the ions at *m/z* 153 and 128 (data not shown) it could be seen that the neutral gain of a molecule of H_2O was a favorable process resulting in a stable ion-H_2O adduct as substantial collision energy (CE minimal 15 eV) was needed to decompose *m/z* 153 and 128. If more than 15 eV was applied, the *m/z* 153 and 128 lost H_2O and again gave rise to *m/z* 135 and 110, respectively.

Repeating this experiment with the $H_2^{18}O$ doped argon as collision gas further indicated the tendency to form these adducts. An $H_2O/H_2^{18}O$ exchange was noticed in the product ion spectra of both in-source

Table 2. Accurate masses and elemental compositions of the product ions following CID of d_3-$[BD_2]^+$, the fully H/D exchanged $[BH_2]^+$ species of guanosine. Their appearance in the product ion spectra of the progenitors of the major pathways is also indicated.

Nominal *m/z*	Theoretical *m/z*	Experimental *m/z*	Mass difference (mDa)	Composition	*m/z* 137	*m/z* 113
157	157.0881	Lock	-	$C_5HD_5N_5O^+$		
156	156.0823	156.0821	−0.2	$C_5H_2D_4N_5O^+$		
155	155.0538	155.0537	−0.1	$C_5H_3D_2N_4O_2^+$	+	
138	138.0495	138.0499	0.4	$C_5HD_3N_4O^+$		
137	137.0432	137.0432	0	$C_5H_1D_2N_4O^+$	Lock	
136	136.0370	136.0374	0.4	$C_5H_2D_1N_4O^+$	+	
131	131.0649	131.0655	0.6	$C_4H_3D_3N_3O_2^+$		+
114	114.0605	114.0604	−0.1	$C_4D_4N_3O^+$		
113	113.0546	113.0543	−0.3	$C_4H_1D_3N_3O^+$		Lock
112	112.0480	112.0477	−0.3	$C_4H_2D_2N_3O^+$		+
109	109.0483	109.0481	−1.7	$C_4H_1D_2N_4^+$	+	
108	108.0420	108.0424	0.4	$C_4H_2D_1N_4^+$	+	
94	94.0152	94.0146	0.6	$C_4D_1N_4O^+$	+	
93	93.0089	93.0092	0.3	$C_4H_1N_4O^+$	+	
86	86.0656	86.0669	1.3	$C_3D_4N_3^+$		+
85	85.0594	85.0598	0.4	$C_3H_1D_3N_3^+$		+
84	84.0531	84.0536	0.5	$C_3H_2D_2N_3^+$		+
82	82.0374	82.0378	0.4	$C_3D_2N_3^+$	+	
81	81.0311	81.0314	0.3	$C_3H_1D_1N_3^+$	+	
80	80.0249	80.0248	−0.1	$C_3H_2N_3^+$	+	
70	70.0374	70.0378	0.4	$C_2D_2N_3^+$	+/−	
69	69.0422	69.0410	−1.2	$C_3H_1D_2N_2^+$		+
	69.0199	69.0201	0.2	$C_3H_1D_1NO^+$	+	
66	66.0202	66.0187	−0.5	$C_3D_1N_2^+$		
65	65.0140	65.0130	−1.0	$C_3H_1N_2^+$	+	
58	58.0485	58.0474	−1.1	$C_2D_3N_2^+$		+
57	57.0422	57.0410	−1.2	$C_2H_1D_2N_2^+$	+	+
56	56.0359	56.0339	−2.0	$C_2H_2D_1N_2^+$		+
54	54.0202	54.0189	−1.3	$C_2D_2N_2^+$	+	
53	53.0140	53.0131	−0.9	$C_2HN_2^+$	+	

generated H_2O adducts (*m/z* 128 and 153), resulting in the formation of ions at *m/z* 130 and 155. In both panels of Figure 5 the presence of typical product ions confirm the interrelationship of the adducted ions with the original fragments found in guanosine.

The absence of any discussion around the formation of H_2O adducts of guanosine in earlier reports might be because in most MS^n studies the parent ion was the upper limit of the *m/z* range covered. Furthermore, from the energy resolved spectra these fragments were most pronounced at lower CE voltages. Earlier reports applied CID conditions which generated a multiplicity of ions but under conditions unfavorable for H_2O adductation.

Gas-phase reactions in the collision cell. The product ions at *m/z* 154 and 136 (cf. Scheme 1) were not yet accounted for in the fragmentations described above. The availability of MS^4 data and accurate mass data together with the knowledge that H_2O was present in the collision cell permitted the tentative assignment of these product ions. The elemental compositions of these ions revealed that they could only be rationalized by a consecutive neutral gain of H_2O followed by a loss of NH_3 or vice versa.

The product ion at *m/z* 154 was seen in the product ion spectra of both $[BH_2]^+$ (*m/z* 152) and *m/z* 135, which linked it to the dissociation pathway of the latter. The elemental composition of *m/z* 154 was $C_5H_4N_3O_3^+$ (calc. *m/z* 154.0253; meas. *m/z* 154.0249), which suggested a second addition of H_2O to *m/z* 135 with a consecutive loss of NH_3. Further support for this neutral gain (H_2O)/neutral loss (NH_3) sequence was provided by the $H_2^{18}O$ doped argon experiments, as product ions at *m/z* 156 and 158 were seen. The accurate mass data led to the respective elemental compositions $C_5H_4N_3^{16}O_2^{18}O^+$ (calc. *m/z* 156.0295; meas. *m/z* 156.0301) and $C_4H_4N_3^{16}O^{18}O_2^+$ (calc. *m/z* 158.0338; meas. *m/z* 158.0336). This confirmed the neutral gain of 2 H_2O molecules (*m/z* 156: $H_2^{16}O$ and $H_2^{18}O$; *m/z* 158: 2*$H_2^{18}O$) and a loss of NH_3.

The presence of *m/z* 136 ($C_5H_2N_3O_2^+$; calc. *m/z* 136.0147; meas. *m/z* 136.0152) was explained by a similar logic; it matched a consecutive neutral gain of H_2O and a neutral loss of NH_3 out of *m/z* 135. Again an extra confirmation was found in the $H_2^{18}O$ experiments as a product ion with *m/z* 138 was observed (calc. *m/z* 138.0189; meas. *m/z* 138.0210).

Interesting product ions at *m/z* 134 and 92, with elemental compositions $C_5H_4N_5^+$ (calc. *m/z* 134.0467; meas. *m/z* 134.0472) and $C_4H_2N_3^+$ (calc. *m/z* 92.0249; meas. *m/z* 92.0262), respectively, appeared in the energy resolved spectra of $[BH_2]^+$. Along the lines of the previous neutral gain/neutral loss concept, their pres-

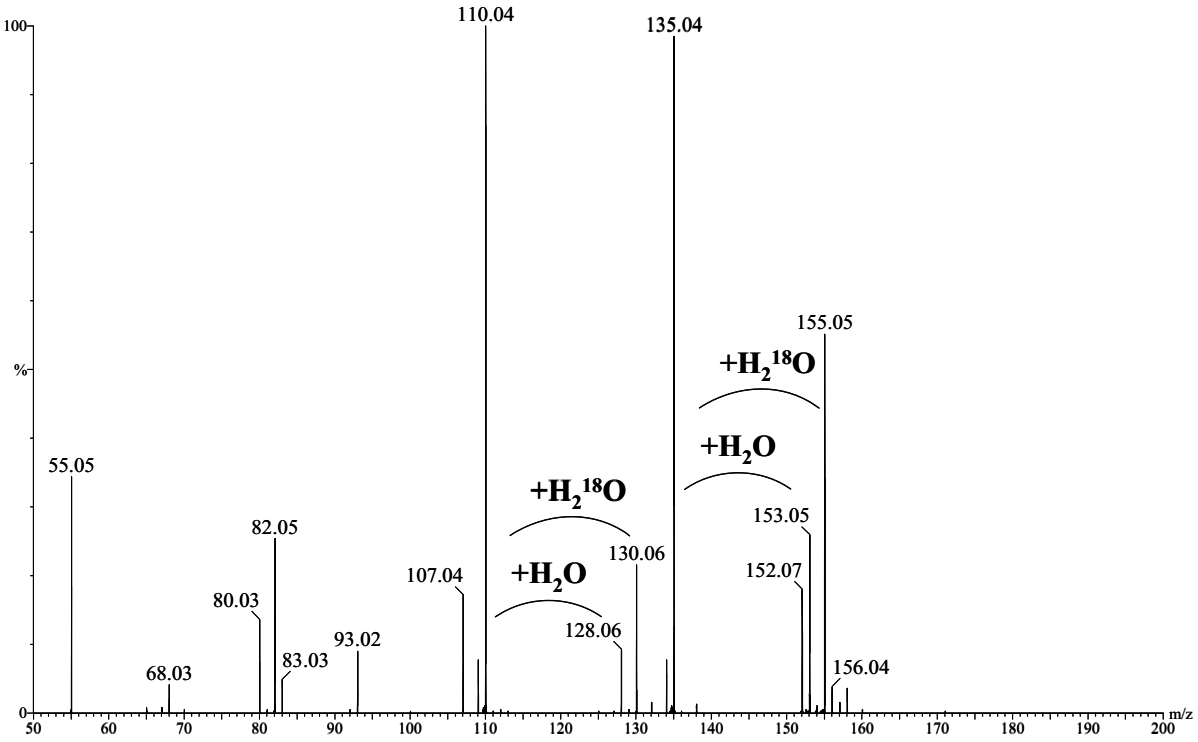

Figure 4. Product ion spectrum of the in-source generated $[BH_2]^+$ ion (*m/z* 152) (CV 40 V and CE 25 eV; no lock mass correction, uncentered). Ar-gas was doped with $H_2^{18}O$.

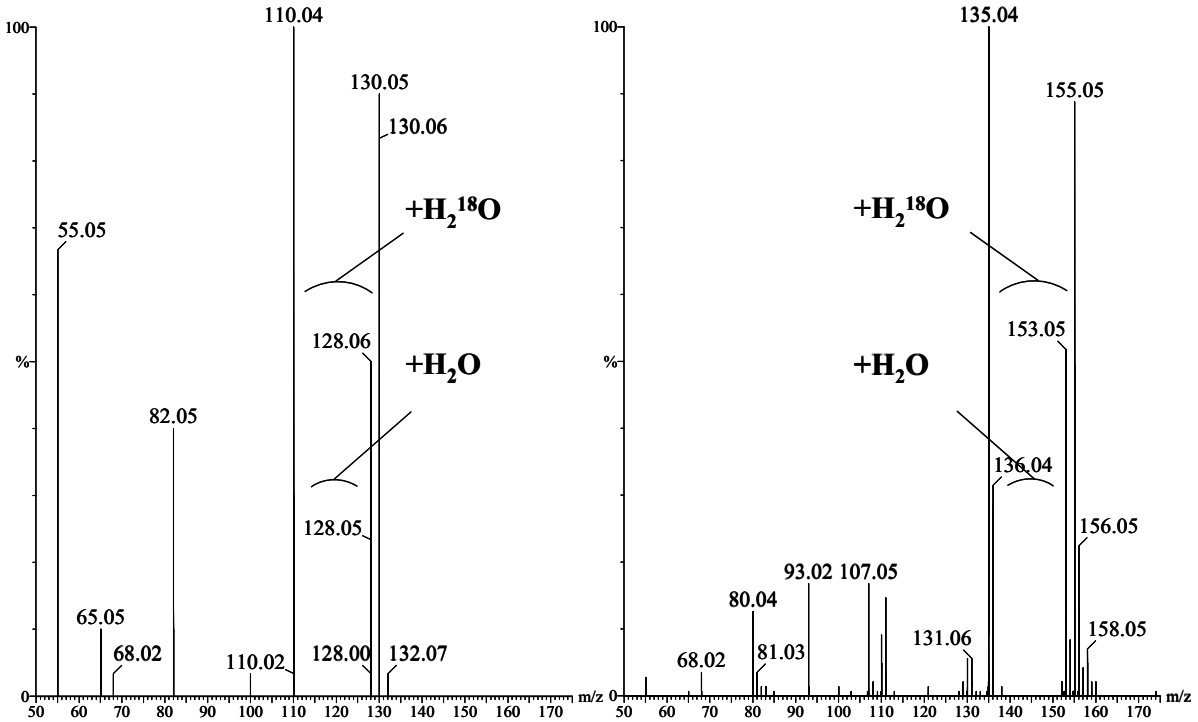

Figure 5. Product ion spectra of the in-source formed H_2O adducts *m/z* 128 (left) and *m/z* 153 (right) of the respective fragments *m/z* 110 and *m/z* 135. The collision gas Ar was saturated with $H_2^{18}O$. (CV 40 V and CE: 20 eV; no lock mass correction, uncentered).

ence could be interpreted as a neutral gain of NH_3 followed by a neutral loss of H_2O out of the fragments *m/z* 135 and 93, respectively. However, this implies the presence of NH_3 in the collision cell. The only known source of NH_3 in these experiments is the NH_3 generated in the deammoniation dissociation pathway of $[BH_2]^+$.

The observation of a neutral gain of H_2O was in agreement with recent *in silico* studies. Chandra et al. and Hanus et al. [15, 17] studied the formation of guanosine mono- and dihydrates in silico and found strong hydrogen bonding stabilizing the different guanosine tautomers. Support for the suggested neutral gain/loss sequences was recently published by Ahn et al.: hydrogen bonding with water molecule(s) significantly reduces the activation barriers for some tautomerization reactions in purine involving a concerted multiple proton mechanism [18]. Such solvent-assisted reactions could explain the remote loss of a neutral NH_3 from the product ion as perceived by us.

In Silico Calculations. It was of interest to compare the experimental results reported above with theoretical data obtained by studying the different ions and their adducts with water using density functional theory (DFT) calculations. To this end, for both the product ions at *m/z* 135 and at 110, geometry optimizations were initiated for the monomer and for the 1:1 adduct. For each fragment, possible geometries were proposed based upon the work of Gregson et al. [24].

For all species, the geometries were optimized using the tight convergence criteria. To ensure that all geometries correspond to minima in the potential energy surface, a force field calculation for each species was carried out in which the vibrational frequencies of the compounds were calculated using the harmonic approximation. In the second step of the calculation, a H_2O molecule was added at a distance ~10 Å away from the ion, and a new geometry optimization was initiated. Also for these species the harmonic frequencies were calculated. In the final step, for both the monomers and the adducts, the internal energy derived from the DFT calculations and the harmonic frequencies were combined and the corresponding values for the enthalpy, the entropy, and the free-energy at room temperature were estimated, using straightforward statistical thermodynamics. The resulting values for the differences ΔH, ΔS, and ΔG describing the formation of the adducts are given in Table 3. Inspection of the equilibrium geometries, also given in Table 3, showed that for both the species at *m/z* 110 and 135, the water molecule is bonded to the ion through a N—H . . . O hydrogen bond. The H . . . O hydrogen bond length obtained for the different complexes is close to 1.6126 and 1.6148 Å, respectively. These values are significantly smaller than the values obtained for hydrogen bonds observed between neutral compounds, which range typically between 1.9 and 2.1 Å [28], and showed that in the adducts the water molecules were much more strongly bonded to the ions. The values also pointed out that the interactions were dominated by electrostatics and in such case the bridging proton tended to drift so far from the proton donor that it became questionable as to which unit was the donor and which was the acceptor [28]. The latter was confirmed by the relative large values obtained for the enthalpy differences ΔH, which were ~2 to 3 times larger than the values obtained for classical hydrogen bonds [28].

If the neutral gain of H_2O by these fragments was a unique feature, this would provide a powerful diagnostic marker to be used in the identification of guanosine nucleosides in complex matrices. To field-test this hypothesis, calculations similar to those obtained for guanosine were also performed for the ions at *m/z* 119 and at 94 observed in the spectra of adenosine, the loss of a NH_3 and a cyanamide out of $[BH_2]^+$, respectively, (Table 3).

However, for these species, a strongly bonded adduct was also predicted by the DFT calculations. The water molecule was bonded either through a N—H . . . O hydrogen bond (*m/z* 119), or through a C—H . . . O hydrogen bond (*m/z* 94). The thermodynamical properties obtained for both adducts compared favorably with the theoretical data obtained for the complexes described above, and will not be discussed here.

It should be noted here that all calculations reported above were performed using density functional theory, while it was known that in such calculations the attractive dispersion forces between the interacting species were not fully accounted for. The complexation energies presented in Table 3, therefore, might be somewhat underestimated. Even if the calculated values were not fully reliable, however, it could safely be concluded that adduct formation should occur in a similar way for both the ions observed in the guanosine and the adenosine spectra.

This indeed is what was observed experimentally: Adenosine was subjected to in-source CID and energy resolved spectra of the ions at *m/z* 109 and 94 were collected with $H_2^{18}O$ doped argon in the collision cell. Although the neutral gain of $H_2^{16}O$ and $H_2^{18}O$ is less pronounced than for the corresponding guanosine fragments, the neutral gain is clear, as illustrated in Figure 6. An uptake of both $H_2^{16}O$ and $H_2^{18}O$ could be observed for both *m/z* 119 and 94, resulting in the respective ions at *m/z* 137 and 139 for the precursor ion *m/z* 119, and *m/z* 112 and 114 for the precursor ion at *m/z* 94.

Further proof was given by the analysis of the in-source formed H_2O adducts. The product ion spectra of the ions at *m/z* 137 and 112 showed the loss of $H_2^{16}O$ and the partial regain of $H_2^{18}O$ by the respective ions at *m/z* 119 and 94.

Both the DFT calculations and the mass spectrometric measurements made clear that the neutral gain of H_2O was not a unique feature of the guanosine frag-

Table 3. Summary of the DFT calculations.

Nominal *m/z*	Adopted fragment structure	B3LYP/6-31 + G(d,p) Equilibrium geometry and thermodynamical properties of the water adducts
110	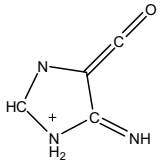	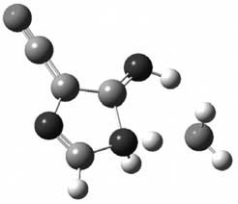
		$\Delta H_{(298K)} = -76.68$ kJ mol^{-1} $\Delta S_{(298K)} = -111.79$ J mol^{-1} K^{-1} $\Delta G_{(298K)} = -43.37$ kJ mol^{-1}
		$K_{eq\ (298K)} = 10^{7.6}$
		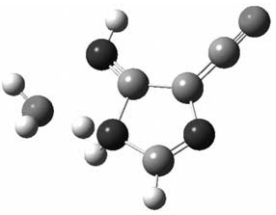
		$\Delta H_{(298K)} = -77.91$ kJ mol^{-1} $\Delta S_{(298K)} = -43.68$ J mol^{-1} K^{-1} $\Delta G_{(298K)} = -44.03$ kJ mol^{-1}
		$K_{eq\ (298K)} = 10^{7.72}$
135	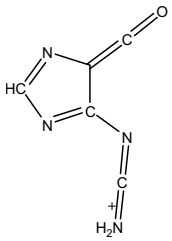	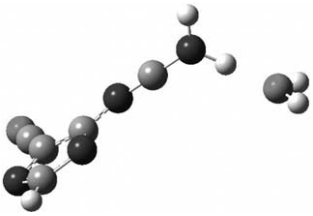
		$\Delta H_{(298K)} = -72.83$ kJ mol^{-1} $\Delta S_{(298K)} = -114.02$ J mol^{-1} K^{-1} $\Delta G_{(298K)} = -39.69$ kJ mol^{-1}
		$K_{eq\ (298K)} = 10^{6.96}$
119	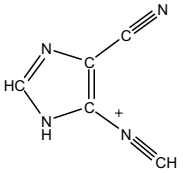	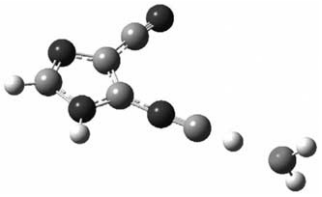
		$\Delta H_{(298K)} = -72.17$ kJ mol^{-1} $\Delta S_{(298K)} = -105.13$ J mol^{-1} K^{-1} $\Delta G_{(298K)} = -40.86$ kJ mol^{-1}
		$K_{eq\ (298K)} = 10^{7.16}$
94	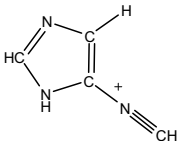	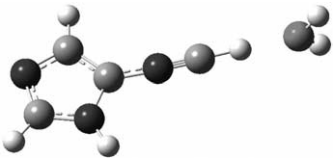
		$\Delta H_{(298K)} = -78.71$ kJ mol^{-1} $\Delta S_{(298K)} = -108.27$ J mol^{-1} K^{-1} $\Delta G_{(298K)} = -46.44$ kJ mol^{-1}
		$K_{eq\ (298K)} = 10^{8.4}$

ments, but can occur for certain fragments of other compounds as well.

The source of H_2O in the collision cell. The question remaining was the origin of H_2O in the collision cell. An instrument-specific default was excluded as this neutral gain of H_2O was observed in the following different instruments: an ion trap MS [8], a triple quadrupole MS, and two different Q-TOF instruments. Furthermore, it was not a site-specific issue either, e.g., following compromised argon-supplies, as the observations were made in both of our mass spectrometric facilities. A search towards the probable cause was carried out on a triple quadrupole instrument (data not shown). When

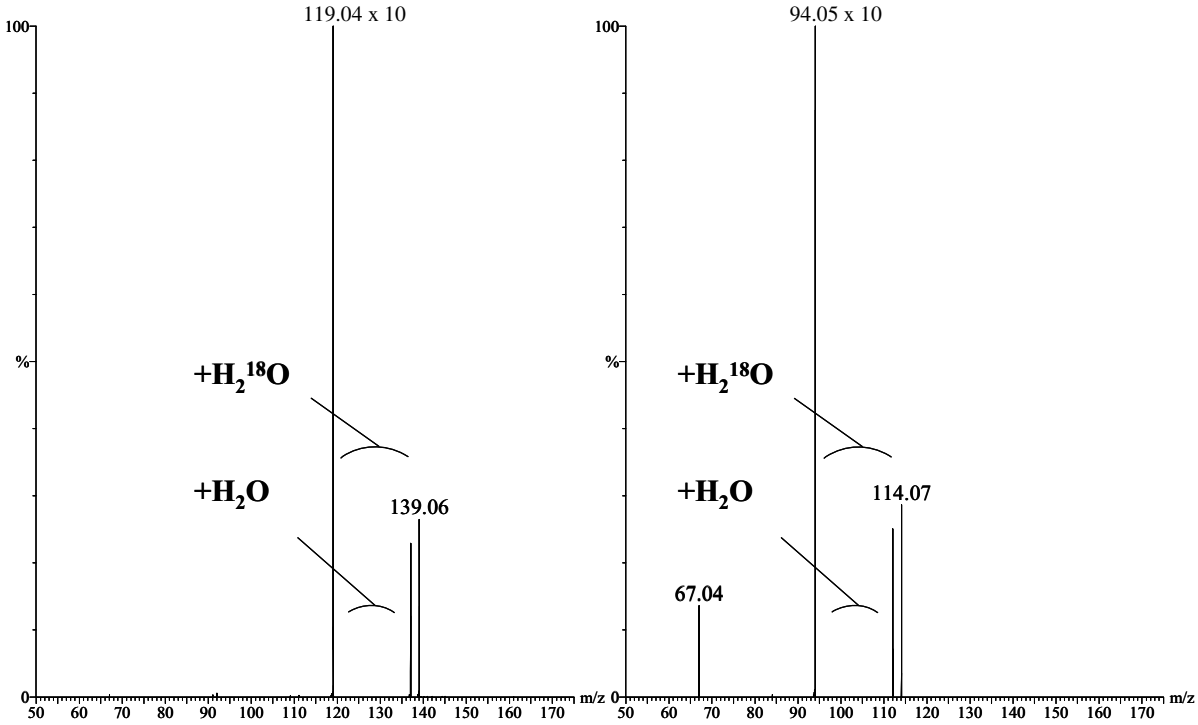

Figure 6. Product ion spectra of the in-source formed *m/z* 119 ions (left) and *m/z* 94 ions (right) of adenosine. Ar-gas was saturated with $H_2^{18}O$. (CV: 80 V and CE: 10eV; no lock mass correction, uncentered).

changing the standard argon supply for the $H_2^{18}O$ doped argon supply it was noticed the $H_2^{16}O$ adducts persisted in the spectra despite the important amounts of $H_2^{18}O$ present (cf. specifications argon in the Experimental section). Only after connecting the $H_2^{18}O$ doped argon supply directly to the collision cell valve, and as such by-passing the stainless steel tubing connecting the gas supply and the actual entrance valve, the $H_2^{18}O$ adducted product ions became more abundant than the $H_2^{16}O$ adducts.

A similar but less pronounced effect was seen on the Q-TOF instrument as it was necessary to flush the gas supply system for about 8 h with the $H_2^{18}O$ doped argon before the $H_2^{18}O$ adducts became more important. All this suggested the stainless steel tubing as the source of the observed H_2O. It was known that substantial amounts of H_2O can adsorb on stainless steel surfaces [29,°30].°This°might°also°explain°the°observations°made on the triple quadrupole instrument: the $H_2^{18}O$ was competing with $H_2^{16}O$ for the active sites on the stainless steel surface and was as such not readily available in the collision cell. By reducing the length of the stainless steel tubing, the presence of $H_2^{18}O$ in the collision was accelerated.

Thus, the relative large internal surface of the stainless steel gas tubing and its sometime considerable lengths (inside and outside the instruments), its high H_2O-adsorbing capacity, and the low flow rates of the collision gas provided a viable explanation of the availability of H_2O in the collision cell for very long periods of time.

Apart from the delivery of H_2O by the collision gas, although being very low (<3 ppm), the contact with the atmosphere during maintenance probably also is a source°of°water°[30].

Although°the°implications of the presence of H_2O in collision cells of tandem MS instruments is not yet fully covered, re-evaluation of other mass spectrometric data revealed similar adduct formation in 6-substituted 3-aminopyridazines [Lemière, unpublished results], suggesting this phenomenon was more common than expected. As demonstrated for the neutral gain of water by *m/z* 135 this can result in product ions at higher *m/z* ratios values than the precursor ion. If only scan ranges below the *m/z* of the parent ion are considered, this can lead to loss of information.

Conclusions

This study demonstrates the potential of Q-TOF instruments for the collection of higher order MS/MS data (MS^4) by optimal usage of in-source CID. Both accurate mass information and clear genealogical relationships of product ions were produced and allowed the unambiguous elucidation of fragmentation pathways. This strategy was field-tested for guanosine and proven powerful; earlier proposed

pathways were completed with new fragments and past uncertainties were clarified.

H_2O uptake in the collision cell by certain product ions of guanosine was demonstrated, based on accurate mass data. These fragment ions were previously reported but not explained. Experiments in which the source of the mass spectrometer was saturated with D_2O/MeOD showed that the water molecules involved in the adduct formation were not originating from the source. At the same time, these spectra gave additional proof for the proposed fragmentation pathways and elemental compositions. Further evidence for a neutral gain of H_2O was acquired by doping the collision gas argon with $H_2^{18}O$. The data also suggested that the availability of H_2O in the collision cell induced more complex gas-phase interactions such as a neutral gain of H_2O followed by a neutral loss of NH_3. This process was observed several times. DFT calculations were implemented to provide insights in the stability and the nature of the H_2O–product ion adducts. Albeit assumptions were made in terms of structures and charge localizations, the computational data proved relevant. Hydrogen bonding came out as being an important stabilizing factor and predictions based on the calculations were experimentally established. The observation of these adducts stress the fact that in-source CID information has to be handled with caution: this adduct-formation also occurs in source concealing/suppressing the actual product ions. A limited discussion about the origins of H_2O in the collision cell was also presented. Adsorption of atmospheric H_2O to the stainless steel tubing often used to supply the collision gas to the instruments is put forward to be the most probable source. Slow desorption of adsorbed H_2O is suggested.

Acknowledgments

The authors gratefully acknowledge funding for this research by a Ph.D. grant of the Institute for the Promotion of Innovation through Science and Technology in Flanders (IWT-Vlaanderen). This research was also funded by the Flemish Foundation for Scientific Research (FWO-Vlaanderen), the Flemish Government (GOA-action), and the University of Antwerp (RAFO).

References

1. Perigaud, C.; Gosselin, G.; Imbach, J. L. Nucleoside Analogs as Chemotherapeutic Agents—A Review. *Nucleosides Nucleotides* **1992,** *11,* 903–945.
2. Gehrke, C. W.; Kuo, K. C.; Waalkes, T. P.; Borek, E. Patterns of Urinary Excretion of Modified Nucleosides. *Cancer Res.* **1979,** *39,* 1150–1153.
3. Borek, E. Modified Nucleosides and Cancer. *Cancer Res.* **1982,** *42,* 2099–2100.
4. Fischbein, A.; Sharma, O. K.; Borek, E. Modified Nucleosides and Early Detection of Occupational Cancer: A Challenge for the Future. *Environ. Med. Notes* **1985,** *52,* 480–483.
5. Schlimme, E.; Boos, K. S.; Frister, H.; Raezke, K.-P.; Wilmers, B. Ribonucleosides: Marker Molecules in Body Fluids. *Fresenius J. Anal. Chem.* **1987,** *327,* 78–79.
6. Limbach, P. A.; Crain, P. F.; McCloskey, J. A. The Modified Nucleosides of RNA—Summary. *Nucleic Acids Res.* **1994,** *22,* 2183–2196.
7. Schram, K. H. Urinary Nucleosides. *Mass Spectrom. Rev.* **1998,** *17,* 131–251.
8. Dudley, E.; Lemiere, F.; Van Dongen, W.; Tuytten, R.; El Sharkawi, S.; Brenton, A. G.; Esmans, E. L.; Newton, R. P. Analysis of Urinary Nucleosides. IV. Identification of Urinary Purine Nucleosides by Liquid Chromatography/Electrospray Mass Spectrometry. *Rapid Commun. Mass Spectrom.* **2004,** *18,* 2730–2738.
9. March, R. E. An Introduction to Quadrupole Ion Trap Mass Spectrometry. *J. Mass Spectrom.* **1997,** *32,* 351–369.
10. Marshall, A. G.; Hendrickson, C. L.; Jackson, G. S. Fourier Transform Ion Cyclotron Resonance Mass Spectrometry: A Primer. *Mass Spectrom. Rev.* **1998,** *17,* 1–35.
11. Chernushevich, I. V.; Loboda, A. V.; Thomson, B. A. An Introduction to Quadrupole Time-of-Flight Mass Spectrometry. *J. Mass Spectrom.* **2001,** *36,* 849–865.
12. Curcuruto, O.; Tarzia, G.; Hamdan, M. Differentiation Between Isomeric Methylated Purine Derivatives by Means of Chemical Ionization and Collision-Induced Dissociation. *Rapid Commun. Mass Spectrom.* **1992,** *6,* 596–600.
13. Kralj, B.; Zigon, D.; Kocjan, D.; Kobe, J. Metastable and Collision-Activated Decomposition of Protonated Molecules of Isomeric N−7- and N−9-substituted purines in the gas phase. *Rapid Commun. Mass Spectrom.* **1997,** *11,* 273–282.
14. Nourse, B. D.; Hettich, R. L.; Buchanan, M. V. Methyl Guanine Isomer Distinction by Hydrogen/Deuterium Exchange Using A Fourier-Transform MassSpectrometer. *J. Am. Soc. Mass Spectrom.* **1993,** *4,* 296–305.
15. Chandra, A. K.; Nguyen, M. T.; Uchimaru, T.; Zeegers-Huyskens, T. Protonation and Deprotonation Enthalpies of Guanine and Adenine and Implications for the Structure and Energy of Their Complexes with Water: Comparison with Uracil, Thymine, and Cytosine. *J. Phys. Chem. A* **1999,** *103,* 8853–8860.
16. Gu, J. D.; Leszczynski, J. Influence of the Oxygen at the C8 Position on the Intramolecular Proton Transfer in C8-Oxidative Guanine. *J. Phys. Chem. A* **1999,** *103,* 577–584.
17. Hanus, M.; Ryjacek, F.; Kabelac, M.; Kubar, T.; Bogdan, T. V.; Trygubenko, S. A.; Hobza, P. Correlated Ab Initio Study of Nucleic Acid Bases and Their Tautomers in the Gas Phase, in a Microhydrated Environment and in Aqueous Solution. Guanine: Surprising Stabilization of Rare Tautomers in Aqueous Solution. *J. Am. Chem. Soc.* **2003,** *125,* 7678–7688.
18. Ahn, D. S.; Lee, S.; Kim, B. Solvent-Mediated Tautomerization of Purine: Single to Quadruple Proton Transfer. *Chem. Phys. Lett.* **2004,** *390,* 384–388.
19. Juliano, V. F.; Gozzo, F. C.; Eberlin, M. N.; Kascheres, C.; doLago, C. L. Fast Multidimensional (3-D and 4-D) MS(2) and MS(3) Scans in a High-Transmission Pentaquadrupole Mass Spectrometer. *Anal. Chem.* **1996,** *68,* 1328–1334.
20. van der Veken, B. J.; Herrebout, W. A. Conformational Characteristics of Methyl Nitrite: A Cryospectroscopic Study. *J. Phys. Chem. A* **2001,** *105,* 7198–7204.
21. Frisch, M. J.; Trucks, G. W.; Schlegel, H. B.; Scuseria, G. E.; Robb, M. A.; Cheeseman, J. R.; Montgomery, J. A., Jr. Vreven, T.; Kudin, K. N.; Burant, J. C.; Millam, J. M.; Iyengar, S. S.; Tomasi, J.; Barone, V.; Mennucci, B.; Cossi, M.; Scalmani, G.; Rega, N.; Petersson, G. A.; Nakatsuji, H.; Hada, M.; Ehara, M.; Toyota, K.; Fukuda, R.; Hasegawa, J.; Ishida, M.; Nakajima, T.; Honda, Y.; Kitao, O.; Nakai, H.; Klene, M.; Li, X.; Knox, J. E.; Hratchian, H. P.; Cross, J. B.; Bakken, V.; Adamo, C.; Jaramillo, J.; Gomperts, R.; Stratmann, R. E.; Yazyev, O.; Austin, A. J.; Cammi, R.; Pomelli, C.; Ochterski, J. W.; Ayala, P. Y.; Morokuma, K.; Voth, G. A.;

Salvador, P.; Dannenberg, J. J.; Zakrzewski, V. G.; Dapprich, S.; Daniels, A. D.; Strain, M. C.; Farkas, O.; Malick, D. K.; Rabuck, A. D.; Raghavachari, K.; Foresman, J. B.; Ortiz, J. V.; Cui, Q.; Baboul, A. G.; Clifford, S.; Cioslowski, J.; Stefanov, B. B.; Liu, G.; Liashenko, A.; Piskorz, P.; Komaromi, I.; Martin, R. L.; Fox, D. J.; Keith, T.; Al-Laham, M. A.; Peng, C. Y.; Nanayakkara, A.; Challacombe, M.; Gill, P. M. W.; Johnson, B.; Chen, W.; Wong, M. W.; Gonzalez, C.; Pople, J. A. *Gaussian 03, Revision C.01*; Gaussian, Inc.: Wallingford CT, 2004.

22. Becke, A. D. Density-Functional Thermochemistry. 3. The Role of Exact Exchange. *J. Chem. Phys.* **1993,** *98,* 5648–5652.
23. Lee, C. T.; Yang, W. T.; Parr, R. G. Development of the Colle-Salvetti Correlation-Energy Formula Into a Functional of the Electron-Density. *Phys. Rev. B* **1988,** *37,* 785–789.
24. Gregson, J. M.; McCloskey, J. A. Collision-Induced Dissociation of Protonated Guanine. *Int. J. Mass Spectrom.* **1997,** *165,* 475–485.
25. Kamel, A. M.; Munson, B. Collision-Induced Dissociation of Purine Antiviral Agents: Mechanisms of Ion Formation Using Gas-Phase Hydrogen/Deuterium Exchange and Electrospray Ionization Tandem Mass Spectrometry. *Eur. J. Mass Spectrom.* **2004**, *10,* 239–257.
26. Frycak, P.; Huskova, R.; Adam, T.; Lemr, K. Atmospheric Pressure Ionization Mass Spectrometry of Purine and Pyrimidine Markers of Inherited Metabolic Disorders. *J. Mass. Spectrom.* **2002,** *37,* 1242–1248.
27. Gabelica, V.; Lemaire, D.; Laprevote, O.; De Pauw, E. Kinetics of Solvent Addition on Electrosprayed Ions in an Electrospray Source and in a Quadrupole Ion Trap. *Int. J. Mass. Spectrom.* **2001,** *210,* 113–119.
28. Scheiner, S. Hydrogen Bonding—A Theoretical Perspective; Oxford University Press: New York, NY, 1997. p 291.
29. Shiokawa, Y.; Ichikawa, M. Measurement and Control of Sticking Probability of H_2O on Stainless Steel Surfaces. *J. Vac. Sci. Technol. A* **1998,** *16,* 1131–1136.
30. Hinkle, L. D. Effect of Purge Pressure on Desorbing Water Removal Rate. *J. Vac. Sci. Technol. A* **2004,** *22,* 1799–1803.